ORIGINAL ARTICLE

Geochemical and isotopic investigation of groundwater mineralization process in the Zeroud basin, central Tunisia

Sarra Bel Hadj Salem · Amor Ben Moussa · Najiba Chkir ·
Kamel Zouari · Anne Laure Cognard-Plancq ·
Vincent Marc · Vincent Valles

Abstract The determination of the origin of the salinity in the Zeroud aquifer (central of Tunisia) and the understanding of its hydrogeological and geochemical behaviors related to severe natural and anthropogenic constraints were approached by the combined survey of major element concentrations and stable isotopes (^{18}O, ^{2}H). The hydrogeochemical investigations of the Zeroud aquifer show that groundwaters can be classified into two major water facies: Ca–SO$_4$–Cl and Na–Cl. The main hydrogeochemical processes that typically control the groundwater mineralization are dissolution of evaporates (halite, gypsum and anhydrite), dedolomitization, cation exchange and mixing processes related to the return flow of irrigation waters and the artificial recharge operations. The stable isotope signatures reveal that the first significant recharge origin is related to the direct infiltration of actual meteoric water particularly observed in the foot of hills bordering the basin and in the vicinity of the Zeroud Wady. A main part of groundwater is significantly affected by evaporation, giving evidence of a recharge mostly from the dam water during the artificial recharge operations. Moderated evaporation of waters was observed in the southern part of the basin, especially in the agricultural areas.

Introduction

In arid and semi-arid regions from North African countries, strategic plans depend entirely on groundwater resources as rainfall is characterized by temporal and spatial variations that are random and sporadic. Consequently, to improve water resources management in these regions, it is important to understand the main process that controls groundwater mineralization. The investigated unconfined aquifer of the Zeroud basin, central Tunisia (Fig. 1), provides drinking and irrigation waters for a major part of the region. During the last decades, this aquifer underwent serious overexploitation, leading to generalized decline of the water table and degradation of groundwater quality. Water supply sustainability is threatened by increasing population, drought and probably by the anthropic features (management), especially in the southern area of the Kairouan plain where the original groundwater quality was poor (Nazoumou 2002; Jeribi 2004; Bel Haj Salem 2006). In spite of the several artificial groundwater recharge operations from reservoir water, a continuous decrease of the water table is still observed downstream in the basin. Moreover, irrigated agricultural areas have been created around the dam reservoir, further enhancing constraints on water storage.

This investigation utilizes a set of geochemical and isotopic tracers intended to elucidate the contribution of

S. B. H. Salem (✉) · A. B. Moussa · K. Zouari
Laboratory of Radio-Analyses and Environment,
National School of Engineers, Sfax, BP 1173,
3038 Sfax, Tunisia
e-mail: sarrabelhajsalem@yahoo.fr

N. Chkir
Department of Geography,
Faculty of Letters and Humanities, Sfax, Tunisia

A. L. Cognard-Plancq · V. Marc · V. Valles
Laboratory of Hydrogéology, Fac. des Sciences,
Univ. Avignon et des Pays de Vaucluse, Avignon, France

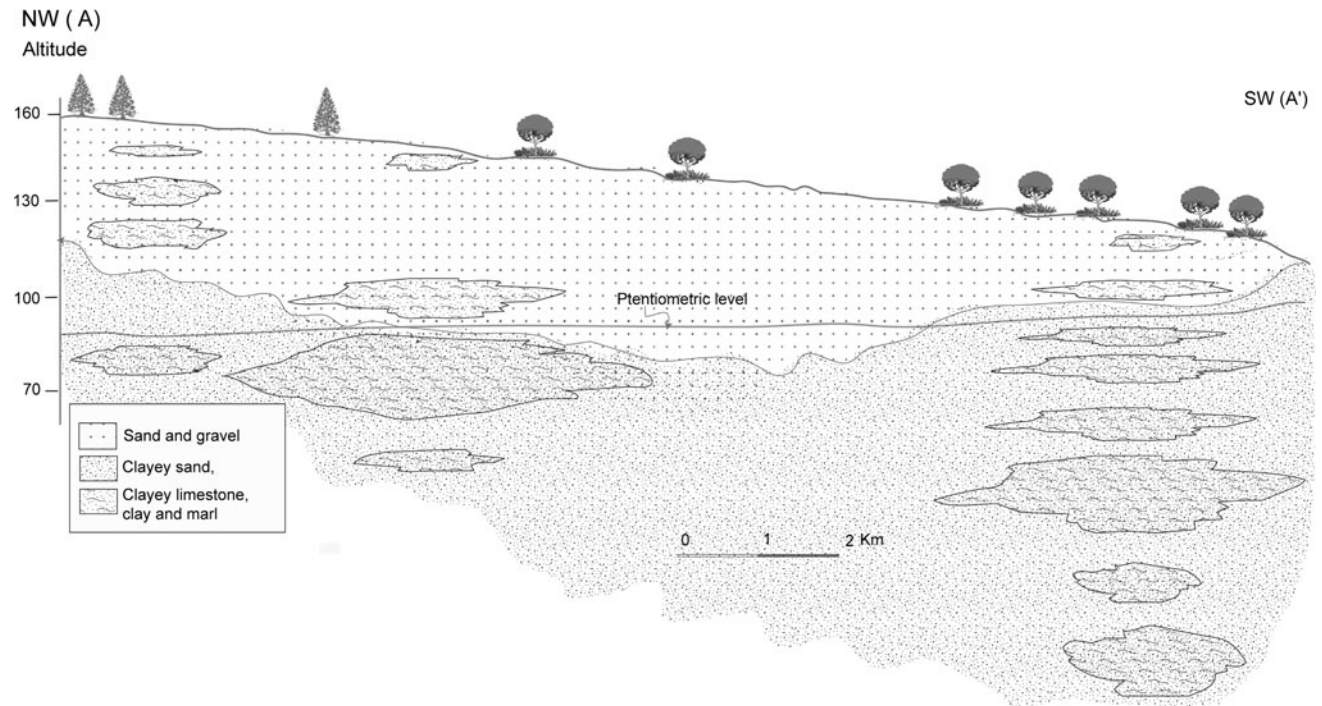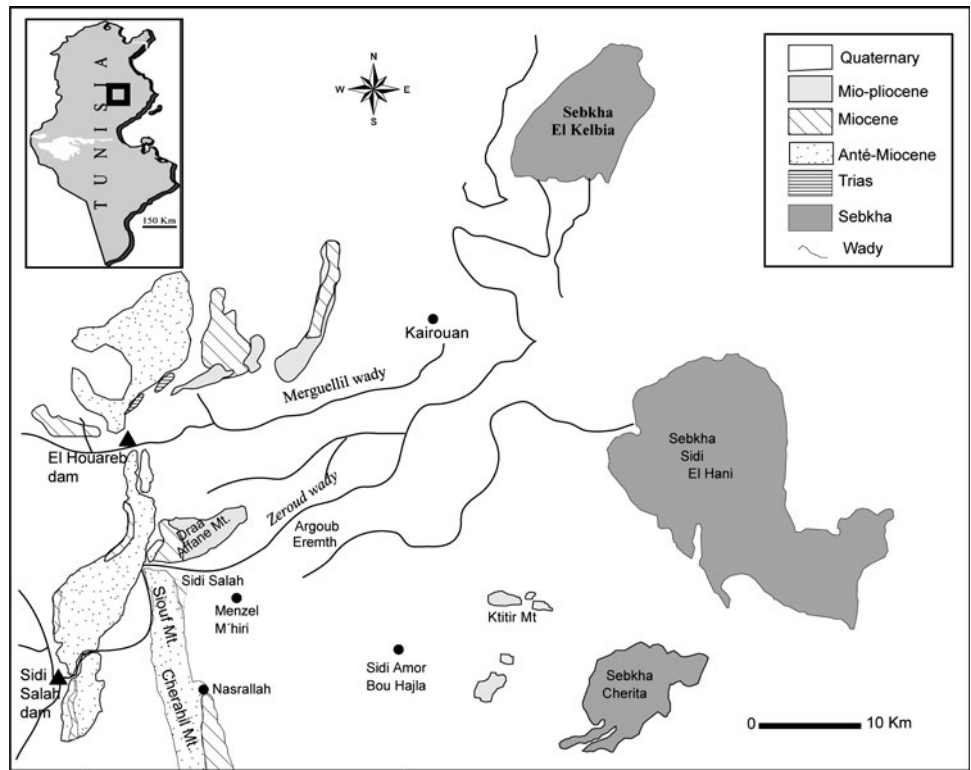**Fig. 1** Location map

Fig. 2 Hydrogeological cross section in the Zeroud unconfined aquifer

the Sidi Saad dam to the recharge of the Zeroud aquifer. In particular, it aims to identify the natural and anthropogenic processes that control groundwater mineralization.

General framework

The Zeroud basin, which encompasses an area extent of about 1,500 km², belongs to the Kairouan plain, in the

central part of Tunisia (Fig. 1). The study area has a semi-arid climate characterized by wet and dry seasons with average annual precipitation, potential evapotranspiration and temperature of 270 mm, 1,600 mm and 20.4°C, respectively. The drainage network is mainly constituted by the Zeroud non-perennial Wady and its effluent. This

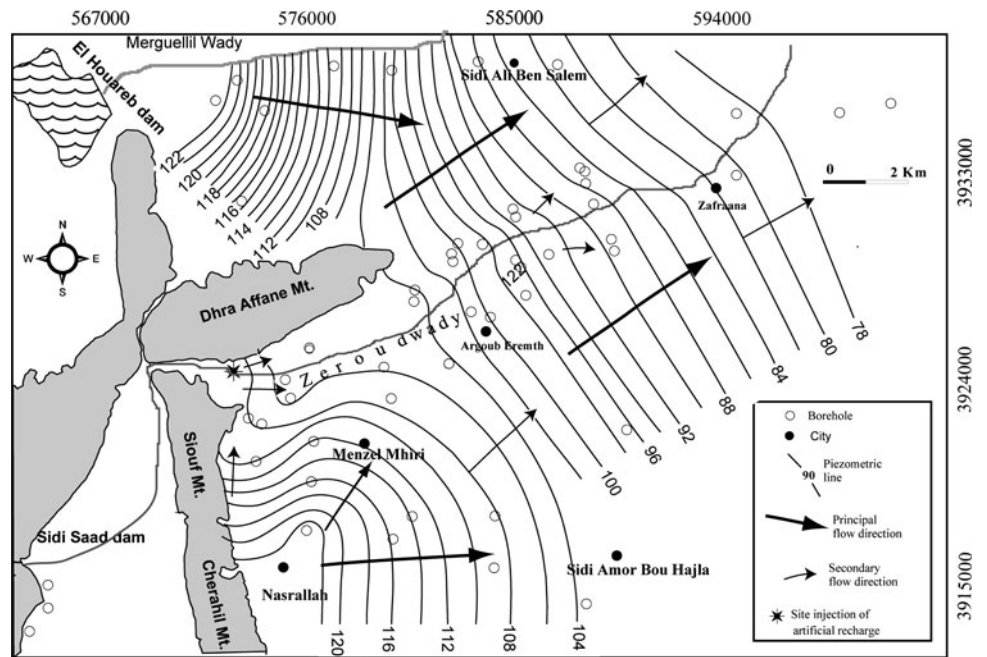Fig. 3 Piezometric map of the Zeroud unconfined aquifer
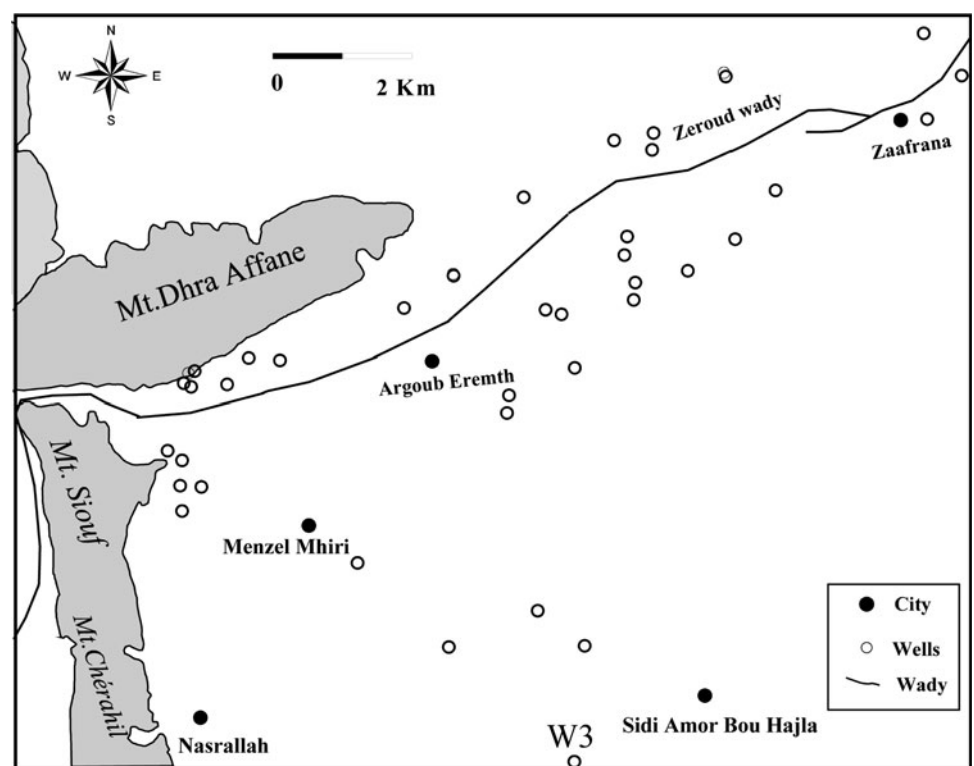

Fig. 4 Sampling map

Table 1 In situ measurements, geochemical and isotopic data of Zeroud basin groundwater

Well number	T (°C)	pH	EC (mS/cm)	TDS (mg/L)	pCO₂	Ca (meq/L)	Mg (meq/L)	Na (meq/L)	K (meq/L)	HCO₃ (meq/L)	CO₃ (meq/L)	CI (meq/L)	SO₄ (meq/L)	NO₃ (meq/L)
W1	19.8	7.4	2.85	2,011.00	−2.40	3.61	6.43	17.08	0.415	2	0	9.95	16.42	0.36
W2	14.2	7.34	3.42	2,175.00	−2.29	3.89	6.75	19.08	0.293	2.4	0	11.2	16.53	0.64
W3	21.4	7.06	6.05	4,072.00	−2.09	12.99	15.36	36.08	0.329	2	0	37.84	20.85	2.51
W4	20.4	7.36	3.26	2,300.00	−2.27	4.68	7.4	18.71	0.406	2.46	0	11.46	18.07	0.59
W5	19.6	7.49	2.72	1,873.00	−2.59	4.83	7.12	14.29	0.433	1.6	0	9.37	17.65	0.77
W6	20.4	7.33	3.16	2,234.00	−2.33	7.76	9.28	15.06	0.401	2	0	12.21	17.32	1.34
W7	19.4	7.23	2.84	2,138.00	−2.40	8.6	9.35	12.49	0.393	1.4	0	14.47	13.94	1.26
W8	19.8	7.15	3.17	2,239.00	−1.99	10.26	10.96	14.81	0	3	0	15.46	15.81	0.66
W9	20.8	7.18	2.75	1,915.00	−2.05	10.69	7	11.04	0.375	2.7	0	10.74	16.59	0.84
W10	18	6.96	3.07	2,253.00	−1.83	10.05	9.22	13.97	0.412	2.8	0	11.14	19.17	0.34
Wll	21.2	7.17	2.68	1,940.00	−2.02	7.72	7.61	12.18	0.386	2.8	0	9.15	17.82	0.23
W12	20	7.28	3.13	2,262.00	−2.21	8.55	10.08	14.64	0.584	2.4	0	13.31	17.09	0.41
W13	17.5	7.33	1.978	1,258.00	−2.13	5.6	5.37	10.08	0.298	3.2	0	7.79	8.72	1.11
W14	20.3	7.4	2.53	1,759.00	−2.25	7.92	6.7	12.22	0.53	2.8	0	8.46	18.37	0.24
W15	20.8	7.3	3.19	2,298.00	−2.16	10.67	10.33	15.55	0.237	2.8	0	13.26	18.33	0.54
W16	13.3	7.61	3.08	2,272.00	−2.51	11.41	8.28	12.84	0.513	2.8	0	9.98	22.93	0.27
W17	18.3	7.24	3.17	2,644.00	−2.29	11.45	14	18.1	0.348	1.9	0	14.5	23.98	0.4
W18	21.4	6.94	2.39	1,580.00	−2.08	6.83	7.51	9.95	0.278	1.4	0	8.43	14.02	0.29
W19	20.4	7.2	2.84	1,851.00	−2.16	5.81	8.45	13.76	0.299	2.2	0	12.15	14.18	0.2
W20	20.6	7.39	2.95	1,956.00	−2.49	6.52	7.37	14.5	0.495	1.6	0	11.38	15.5	0.6
W21	16.4	7.55	3.16	2,182.00	−2.19	10.17	10.68	12.89	0.066	3.2	0	11.98	16.05	0.37
W22	18.7	7.32	2.68	1,909.00	−2.14	8.86	8.14	13.38	0.443	2.8	0	9.6	17.27	0.21
W23	21.5	7.3	2.75	1,852.00	−2.12	4.73	5.55	18.49	0.292	2.79	0	10.22	13.33	0.06
W24	20.8	7.48	1.299	820.00	−2.57	1.96	1.93	9.38	0.127	4.2	0	3.57	4.26	0.19
W25	20.9	7.41	2.93	1,975.00	−2.42	8.42	8.88	14.76	0.385	1.4	0	11.35	17.54	0.33
W26	20.00	7.53	4.23	3,121.00	−2.49	20.91	10.61	20.75	0.499	2.8	0	22.07	23.18	0
W27	19.30	7.62	4.42	3,319.00	−2.36	20.34	10.83	25.72	0.603	3	0	28.12	22.16	0.18
W28	20.90	7.54	2.80	2,034.70	−1.83	10.43	7.37	14.93	0.347	3.08	0	12.42	13.77	0.64
W29	21.60			2,308.00	−2.56	11.26	10.66	14.37	0.007	3	0	14.12	16.89	0.8
W30	23.90	7.72	3.93	2,917.00	−2.62	18.72	8.04	21.85	0.476	3	0	18.43	23.06	0.08
W31	16.40	7.73	1.88	1,417.00	−1.88	7.55	4.61	8.78	0.218	2.7	0	5.21	11.74	0.29
W32	20.30			2,371.00	−2.51	13.66	8.68	16.48	0.09	2.7	0	14.57	20.4	0.34
W33	19.80	7.55	3.00	2,262.00	−2.55	11.88	9.04	14.21	0.501	2.3	0	11.58	19	0.13
W34	19.80	7.71	4.42	3,194.00	−1.87	16.1	11.43	28.87	0.675	3.2	0	28.14	20.83	0.1
W35				2,664.00	−1.90	11.6	12.85	17.39	0.682	2.6	0	16.99	21.6	0.71
W36				2,083	−1.88	8.33	8.12	15.32	0.377	2.4	0	14.08	14.65	0.7
W37				3,248	−1.90	15.26	10.35	24.36	0.515	2.6	0	20.43	23.15	1.39
W38				2,209	−1.99	11.14	7.79	15.56	0.435	2.4	0	14.04	15.61	0.68
W39				3,039	−1.95	16.94	10.12	19.66	0.425	2	0	18.69	22.39	0.6
W40				3,073		16.53	9.26	20.75	0.524	2.2	0	19.97	23.34	0.07

Well number	(‰ vs. SMOW)		SI					
	¹⁸O	²H	Calcite	Aragonite	Dolomite	Gypsum	Anhydrite	Halite
W1	−6.05	−37.50	−0.47	−0.61	−1.19	−1.05	−1.28	−5.50
W2	−5.77	−35.72	−0.50	−0.65	−1.37	−1.01	−1.26	−5.39
W3	−5.12	−34.82	−0.32	−0.46	−1.04	−0.61	−0.84	−4.64
W4	−5.34	−36.35	−0.31	−0.46	−0.93	−0.93	−1.17	−5.40
W5	−5.62	−37.32	−0.36	−0.51	−1.06	−0.90	−1.14	−5.60
W6	−5.27	−35.32	−0.21	−0.36	−0.84	−0.75	−0.99	−5.47
W7	−5.78	−36.76	−0.41	−0.56	−1.30	−0.78	−1.02	−5.47

Table 1 continued

Well number	(‰ vs. SMOW)		SI					
	^{18}O	^{2}H	Calcite	Aragonite	Dolomite	Gypsum	Anhydrite	Halite
W8	−5.64	−35.39	−0.10	−0.25	−0.68	−0.69	−0.93	−5.38
W9	−5.76	−35.83	−0.08	−0.22	−0.83	−0.62	−0.85	−5.66
W10	−5.98	−35.41	−0.37	−0.52	−1.31	−0.61	−0.85	−5.54
Wll	−5.12	−29.31	−0.21	−0.36	−0.92	−0.72	−0.95	−5.69
W12	−5.36	−38.47	−0.15	−0.29	−0.73	−0.72	−0.96	−5.45
W13	−5.55	−35.52	−0.10	−0.25	−0.76	−1.04	−1.28	−5.81
W14	−5.33	−35.08	0.01	−0.14	−0.55	−0.69	−0.93	−5.72
W15	−5.80	−37.03	0.03	−0.11	−0.44	−0.63	−0.86	−5.43
W16	−4.46	−30.79	0.24	0.09	−0.28	−0.48	−0.73	−5.62
W17	−5.40	−33.42	−0.24	−0.39	−0.92	−0.53	−0.77	−5.33
W18	−5.95	−36.47	−0.75	−0.90	−1.95	−0.83	−1.06	−5.80
W19	−5.31	−33.28	−0.39	−0.54	−1.13	−0.92	−1.15	−5.51
W20	−4.79	−35.12	−0.30	−0.45	−1.05	−0.83	−1.07	−5.51
W21	−5.44	−38.48	0.28	0.13	0.00	−0.67	−0.91	−5.54
W22	−5.99	−35.36	−0.04	−0.19	−0.64	−0.68	−0.92	−5.62
W23	−5.22	−36.48	−0.26	−0.41	−0.93	−1.00	−1.24	−5.45
W24	−5.17	−36.22	−0.15	−0.30	−0.80	−1.65	−1.88	−6.16
W25	−5.48	−36.04	−0.24	−0.39	−0.95	−0.71	−0.94	−5.51
W26	−5.00	−33.00	0.49	0.34	0.18	−0.33	−0.57	−5.10
W27	−4.89	−32.48	0.58	0.43	0.37	−0.37	−0.61	−4.91
W28	−5.55	−37.81	0.34	0.19	0.04	−0.71	−0.94	−5.47
W29	−5.13	−31.39	−0.19	−0.34	−0.89	−0.64	−0.87	−5.44
W30	−4.01	−29.82	0.71	0.57	0.62	−0.37	−0.59	−5.16
W31	−6.10	−42.31	0.32	0.17	−0.15	−0.80	−1.05	−6.04
W32	−5.10	−37.10	−0.20	−0.34	−1.09	−0.49	−0.73	−5.37
W33	−4.62	−28.03	0.23	0.08	−0.17	−0.56	−0.79	−5.52
W34	−4.87	−31.20	0.61	0.46	0.56	−0.49	−0.72	−4.86
W35	−5.88	−34.25	−0.23	−0.38	−0.85	−0.58	−0.80	−5.29
W36	−5.91	−37.62	−0.35	−0.49	−1.14	−0.79	−1.01	−5.41
W37	−4.23	−27.63	−0.13	−0.28	−0.86	−0.46	−0.68	−5.08
W38	−5.42	−34.27	−0.23	−0.38	−1.05	−0.66	−0.88	−5.41
W39	−3.36	−22.35	−0.19	−0.33	−1.03	−0.42	−0.64	−5.20
W40	−5.96	−37.14	−0.17	−0.31	−1.01	−0.41	−0.63	−5.15

Wady collects the surface runoff from the surrounding hills, close to the Algerian border, toward Sebkhet Kelbia (Bouzaiane and Laforgue 1986).

Geology and hydrology

According to the geological map (Fig. 1), the oldest outcrops in the study area are the deposits of cretaceous age. These Eocene–Oligocene series are found in the surrounding mountains of Jebel Cherahil and Siouf. Limestone and marly limestone deposits of Neocene are located in Draa Affane. Inside the plain, quaternary deposits are represented by alluvial and crusts limestone. These deposits are covered by an eroded quaternary fluvial crust of variable thickness composed mainly of coarse sand (Bedir 1995; Yaich 1984).

The hydrogeologic cross section shows that the plio-quaternary continental detrital deposits constitute an important aquifer system. The aquifer mainly consists of sands, clayey sands and sandstones, with dominant lenticular levels of clay and sandy clayey (Fig. 2). The upper part of this aquifer system is logged in the sandy level and is taped by 5,000 wells with a depth ranging from 20 to 30 m (wells in the Kairouan plain). The intermediate and the lower parts are taped by several deep boreholes with a maximum depth of 500 m. These superposed aquifers are

separated by semi-permeable levels, which increase in thickness and frequency from west to east. In the central part of the plain, communication and admixture between groundwater levels seem possible (Dassi 2004).

The groundwater flow is mainly SW–NE from Cherahil and Siouf mountains towards the Sebkhet Kelbia depression that conforms to the Merguellil and Zeroud Wadis flow paths (Fig. 3). In the western part of the basin, secondary flow directions diverge from the Zeroud Wadi, highlighting the significant contribution of this wady to the aquifer system recharge. The southern part of the basin, especially in the Menzel Mhiri area, is distinguished by convergent flow directions, which indicate a local recharge of the aquifer system. This may indicate the significant contribution of the return flow of irrigation, in relation with agricultural activities, to the aquifer recharge and/or the infiltration of rainfall in the foot of Chérahil maintain.

Chemical and isotopic analyses

A total of 40 wells were sampled for geochemical and isotopic analyses in March 2008 (Fig. 4). Groundwater samples were filtered (0.45 μm) and collected in polyethylene bottles for major elements analysis, which was done at the Laboratory of Radio-Analyses and Environment (LRAE) of the National School of engineers of Sfax (Tunisia), using titration method (for HCO_3) and standard ion chromatography techniques. The liquid-ion chromatography (HPLC) was performed using a Waters chromatograph equipped with columns IC-PakTM CM/D for cations, using EDTA and nitric acid as eluent, and on a Metrohm chromatograph equipped with columns CI SUPER-SEP for anions using phthalic acid and acetonitric as eluent. The overall detection limit for ions was 0.04 mg/l.

Hydrogen and oxygen isotopes analyses were performed in March 2008 for samples from 40 wells. These analyses were carried out in the laboratory of the International Agency of Atomic Energy in Vienna (IAEA) using, respectively, reduction of water on zinc and equilibration with CO_2 gas (Epstein and Meyada 1953). Then they were analyzed by mass spectrometry in which the difference between the sample and the standard Vienna-standard mean oceanic water (VSMOW) is determined. This deviation is presented in the standard δ-notation as per mil (‰) and defined as:

$$\delta^{18}O \ (\permil) = \left[\left(^{18}O/^{16}O \right)_{sample} - \left(^{18}O/^{16}O \right)_{standard} \right] 1{,}000/ \left[\left(^{18}O/^{16}O \right)_{standard} \right] \quad (1)$$

The V-SMOW standard has an $^{18}O/^{16}O$ isotopic ratio of $(2005.2 \pm 0.45) \times 10^{-6}$ (Beartschi 1976). The measurement precision for stable isotope analysis is about

of ±0.15‰ for oxygen-18 and ±2‰ for deuterium. During this period, 29 measurements of tritium were conducted (Table 1). Tritium analyses were carried out in the Laboratory of Avignon (France) by electrolytic enrichment and liquid scintillation counting method (Thatcher et al. 1977). Tritium contents were presented in tritium unit (TU), in which one TU equals one tritium atom per 10^{18} hydrogen atoms.

Results

Partial pressure carbon dioxide (pCO_2), calculated with PHREEQC program (Parkhurst and Appelo 1999), in situ measurements data and chemical analyses of 40 wells samples tapping the Zeroud aquifer system are represented in Table 1. Log (pCO_2) values range from −2.5 to −1.7. This range is known to relate to water residence time. The low end is typical for recent and surface waters and the high end is reported in literature for old waters with a longer residence time (Parkhurst and Appelo 1999).

To distinguish the different waters types in the studied aquifer system, major ions were plotted on the Piper trilinear diagram (piper 1944) (Fig. 5). Groundwater samples can be classified into two major groundwater groups. The first group corresponds to the Na–Cl–SO_4 facies, which is located downstream and in the southern part of the basin. The second group corresponds to the Ca–SO_4–Cl facies with total mineralization values averaging around 2,000 mg l^{-1}. The results show variation of groundwater salinity, represented by the TDS values, ranging from less than 1 g/l to almost 4 g/l.
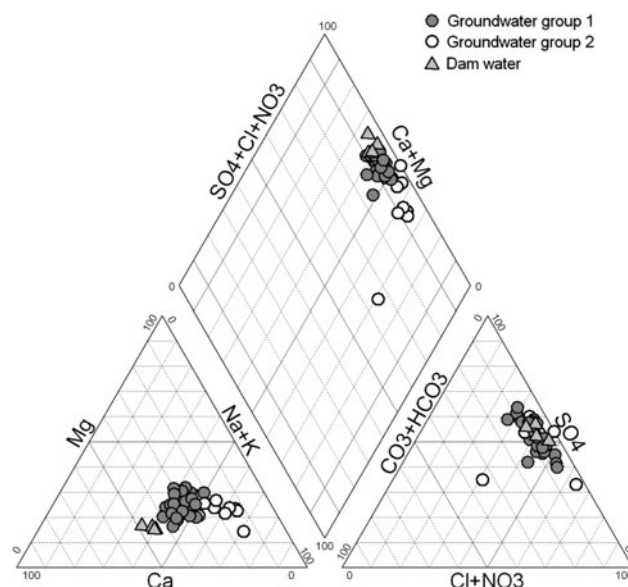

Fig. 5 Piper diagram of the Zeroud aquifer

The average $\delta^{18}O$ and $\delta^{2}H$ compositions of the Zeroud aquifer are about -5.6 and $-34.6‰$, respectively. The pattern obtained from the $\delta^{18}O$ and $\delta^{2}H$ values is similar to that previously reported by Jeribi 2004.

Discussion

Geochemical study

Partial pressure carbon dioxide (pCO2)

Spatial distribution of log (pCO2) during March 2008 (Fig. 6) clearly indicates that the high contents are related to old waters. However, the low values characterize the recharge area. Three types of groundwater are distinguished: (1) fresh groundwater with lower pCO2 levels upstream the plain close to the injection site of the artificial recharge and near the Zeroud Wady. This could be explained by the influence of the artificial recharge operations and the native recharge along the Wady course; (2) groundwater with higher pCO2 levels reflecting longer residence times in the central part and the downstream of the basin, which provide insight into the more extensive reactions with aquifer minerals and microbial mediated reactions that produce CO2. (3) Mixed groundwater with low pCO2 values located in the largely irrigated zone such as Menzel Mhiri region. The pCO2 values fluctuate slightly from a month to another, according to the exploitation. In

fact, in the irrigated area, the return flow of irrigation water is strongly suggested, considering the relatively low depth of the shallow aquifer water table in the mentioned region.

Major elements geochemistry

The spatial distribution conforms partially with the main groundwater flow direction, indicating that the groundwater salinity is in some way controlled by the residence time in the aquifer. Relatively low TDS values characterize wells located near the Zeroud River and reveal the dilution of groundwater by the water from linear recharge (Fig. 7). However, high values of TDS which relatively disturb the evolution of the mineralization in the direction of the groundwater flow appear near the Draa Affane Mountain, which can be related to evaporates rich-minerals cropping out in this region and leached by Zeroud Wady. Furthermore, high salinity was observed also in the south of the basin, especially in Menzel Mhiri region which is marked by extensive land use development activities.

Nitrate values in the Zeroud basin vary in a wide range from 0 to 150 mg/l. The majority of groundwater samples, particularly those collected from the Menzel Mhiri agricultural region, have nitrate concentrations exceeding 50 mg/l, which represents the maximum European admissible nitrate concentration in drinking water. The spatial distributions of NO3 and TDS display practically the same evolution, highlighting the significant contribution of nitrate to the groundwater mineralization. Furthermore, the

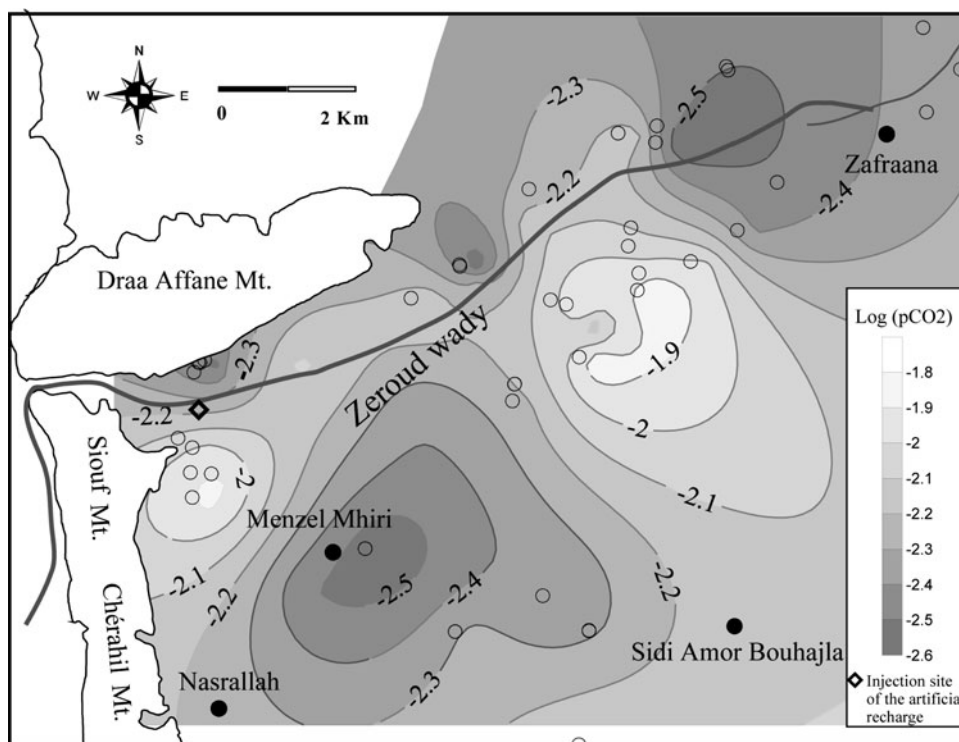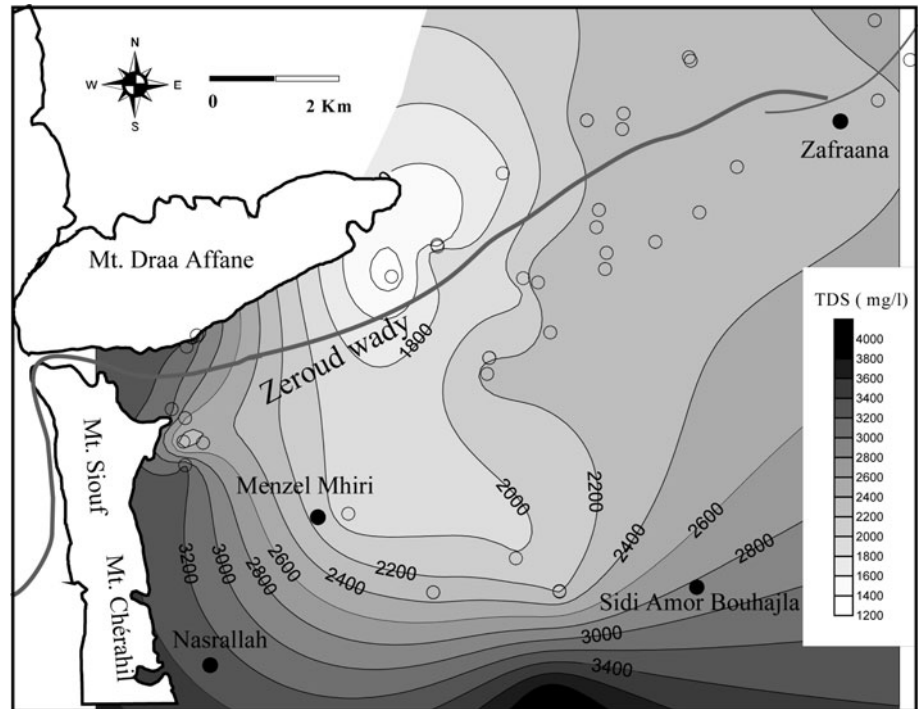Fig. 6 Spatial distribution of log (pCO2)
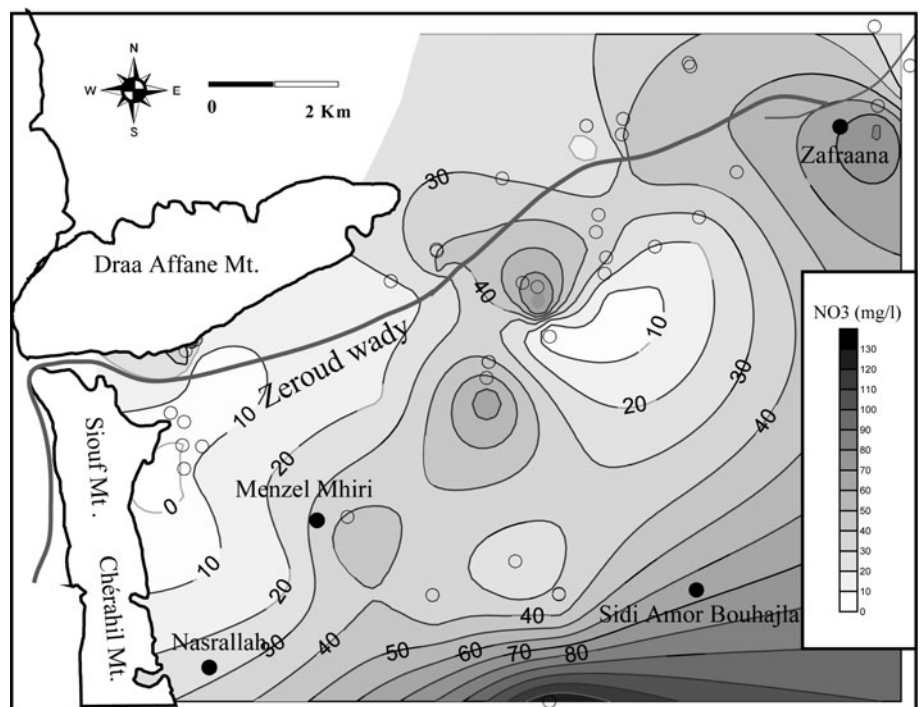
Fig. 7 Spatial distribution of TDS

inspection of the nitrate distribution clearly indicates that highest values are related to the agricultural land use patterns (Fig. 8). This suggests that the applications of nitrogen fertilizers in Menzel Mhiri agricultural region lead to increased nitrates leaching with concentrations up to 50 mg/l. Indeed, this increase of nitrate contents in groundwater during the last decade is also observed in the

Mergullil basin (northern part of the Kairouan plain) (Ben Ammar 2007).

On the other hand, plots of major elements as a function of TDS values were established to determine the contributing elements to groundwater mineralization and the major hydrogeochemical processes. These plots show that there is a well-defined correlation between Na, Cl, Ca, Mg and SO_4 on

Fig. 8 Spatial distribution of NO_3
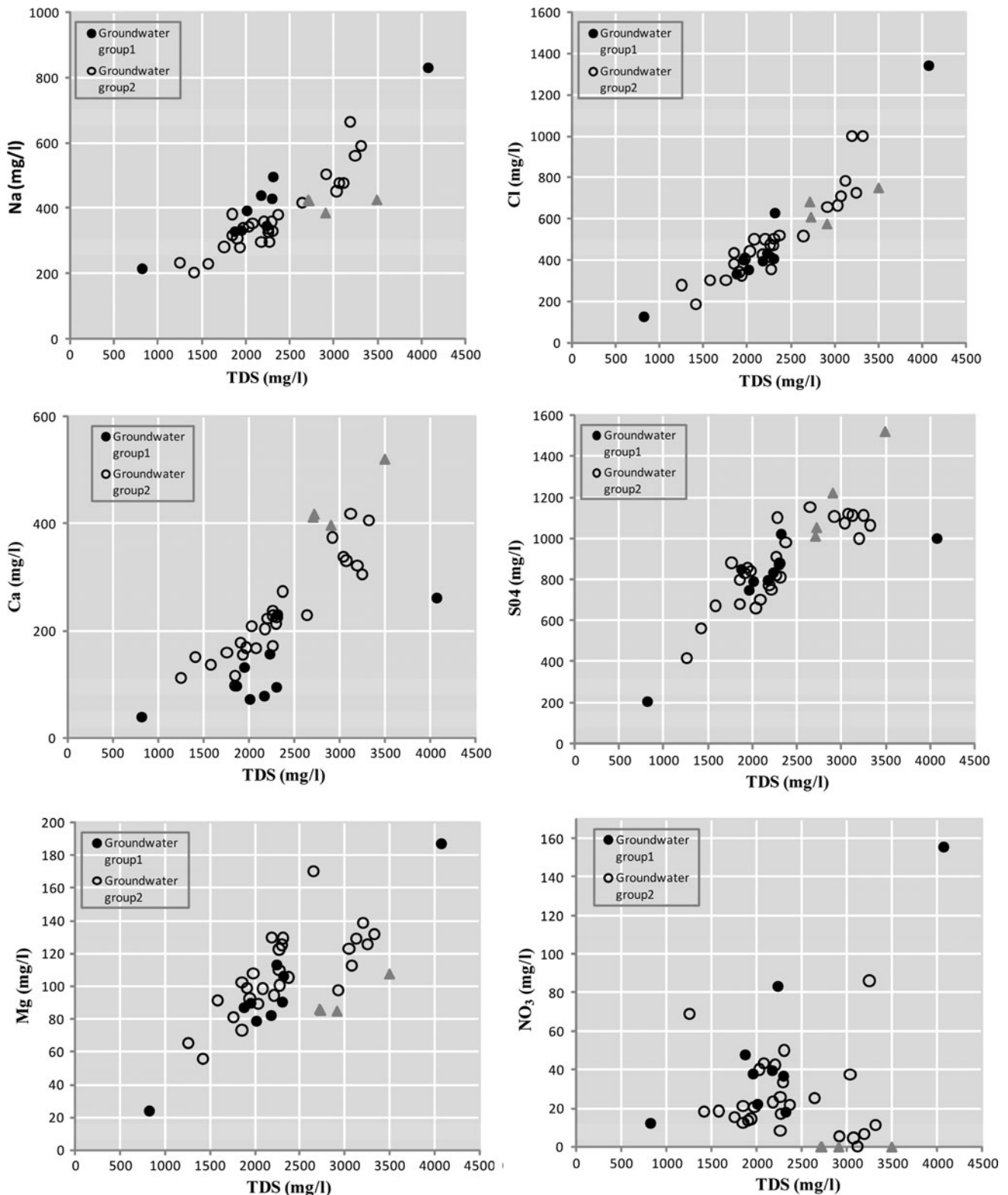
Fig. 9 Major elements and Nitrate versus TDS relationships

one hand and the TDS on the other hand, suggesting that the referred ions are the main contributors to groundwater mineralization (Fig. 9). Moreover, the spatial distributions of the mentioned elements and TDS values show particularly the same evolution, which confirms their participation to the salinization processes (Fig. 10).
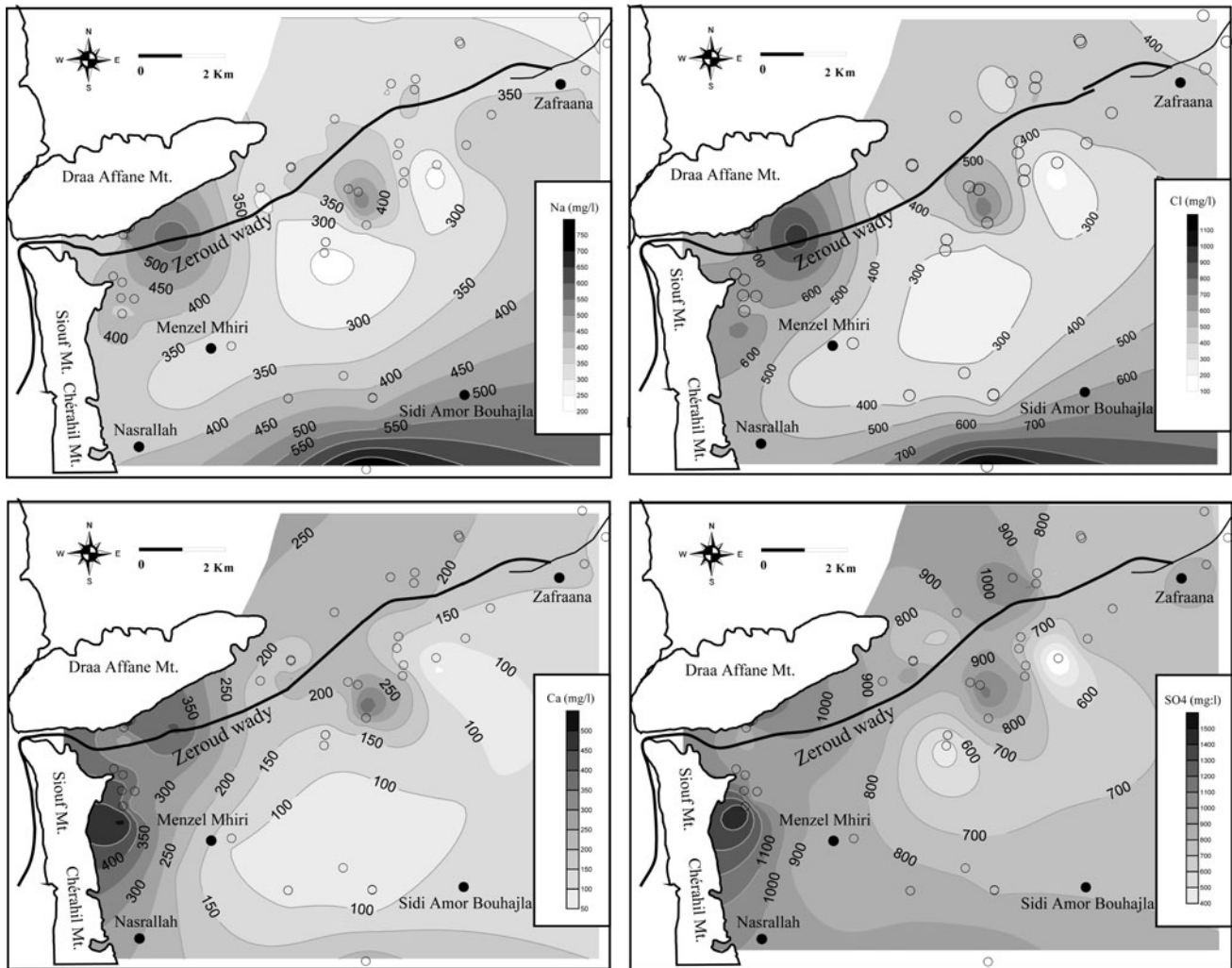
Fig. 10 Spatial distribution of Na, Cl, Ca, SO$_4$

The Na/Cl relationship (Fig. 11) shows that the majority of samples fall on the line 1:1 (Na:Cl) line. This well-defined relationship and the relatively high concentrations in Na and Cl ions corroborate with the role of halite dissolution as an important process contributing to the groundwater salinization in the Zeroud basin (Appelo and Postma 1993). Firstly, this dissolution is verified through the general increasing trend in the Na and Cl concentrations along the groundwater flow direction (Fig. 10); secondly, by the proportional correlation between (Na + Cl) and the negative saturation indexes, which indicates an undersaturation state of groundwater with respect to the halite (Fig. 11).

Some groundwater samples are undersaturated with respect to gypsum and anhydrite and plot along a linear trend in the Ca/SO$_4$ relationship (Fig. 11). These saturation indexes, which vary proportionally to the sum of Ca and SO$_4$, confirm that the dissolution of the above-mentioned sulfate minerals are additional dominant mineralization

processes. The relative excess of SO$_4$ with respect to Ca, identified in the plot of Ca versus SO$_4$ (Fig. 11), suggests that there is another supplementary mineralization process, probably related to the modification by reverse cation exchange phenomenon. During this process, Ca^{2+} in the solution is exchanged with Na$^+$ previously absorbed on the surface of clay minerals in the aquifer matrix. The referred ions exchange is confirmed through the relationship illustrated in Fig. 12, in which (Na–Cl) and [(SO$_4$ + HCO$_3$) − (Ca + Mg)] vary proportionally (Carol et al. 2009). Additionally, the dam water, which is intensively used for irrigation practices, is characterized by high sulfates contents and can contribute to the increase of this element in groundwater.

In the Zeroud basin, groundwaters are undersaturation with respect to sulfate minerals (gypsum and anhydrite) and in equilibrium with respect to carbonate minerals (calcite and dolomite). As calcite precipitates, the concentration of bicarbonate decreases in groundwaters, which
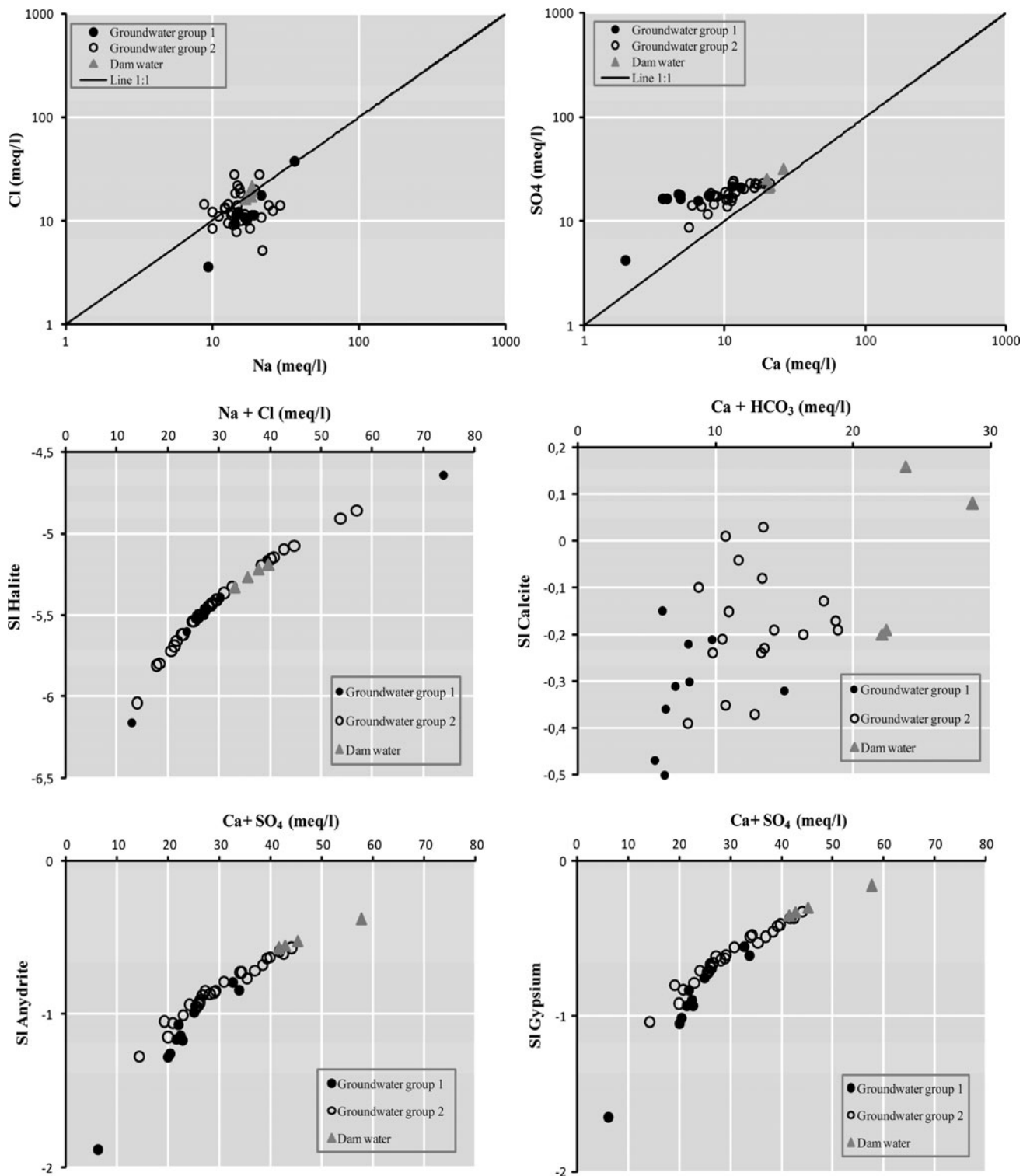
Fig. 11 Plots of Na versus Cl, Ca versus SO$_4$, (Na + Cl) versus SI of halite, (Ca + SO$_4$) versus SI of Anhydrite, (Ca + SO$_4$) versus SI Gypsum, (Ca + HCO$_3$) versus SI Calcite

causes the undersaturation with respect to dolomite and enhances the incongruent dissolution of this mineral known as dedolomitization (Appelo and Postma 1993). As the

reaction proceeds in groundwaters, Ca/Mg ratio decreases and sulfate concentration increases according to the following reaction (Mokrik and Petkevièius 2002):

Fig. 13 $\delta^{18}O/\delta^{2}H$ diagram

On the plot of [Ca + Mg] versus [SO$_4$ + 0.5 HCO$_3$], the dedolomitization reaction yields a straight line with a slope of 1 (Fig. 12).

The examination of the SO$_4$/Cl exhibits a clear relationship between these two elements, which may reflect the degree of mixing between fresh and saltwater in the groundwaters of the Zeroud aquifer. Higher SO$_4$/Cl ratio indicates a long-term water–rock interaction, which permits the dissolution of small gypsiferous fractions dispersing throughout the aquifer. This relatively prolonged water–rock interaction is most likely due to the lower hydraulic conductivity and transmissivity of the aquifer formation. Groundwater samples (Fig. 12) marked by higher SO$_4$/Cl ratio are located in t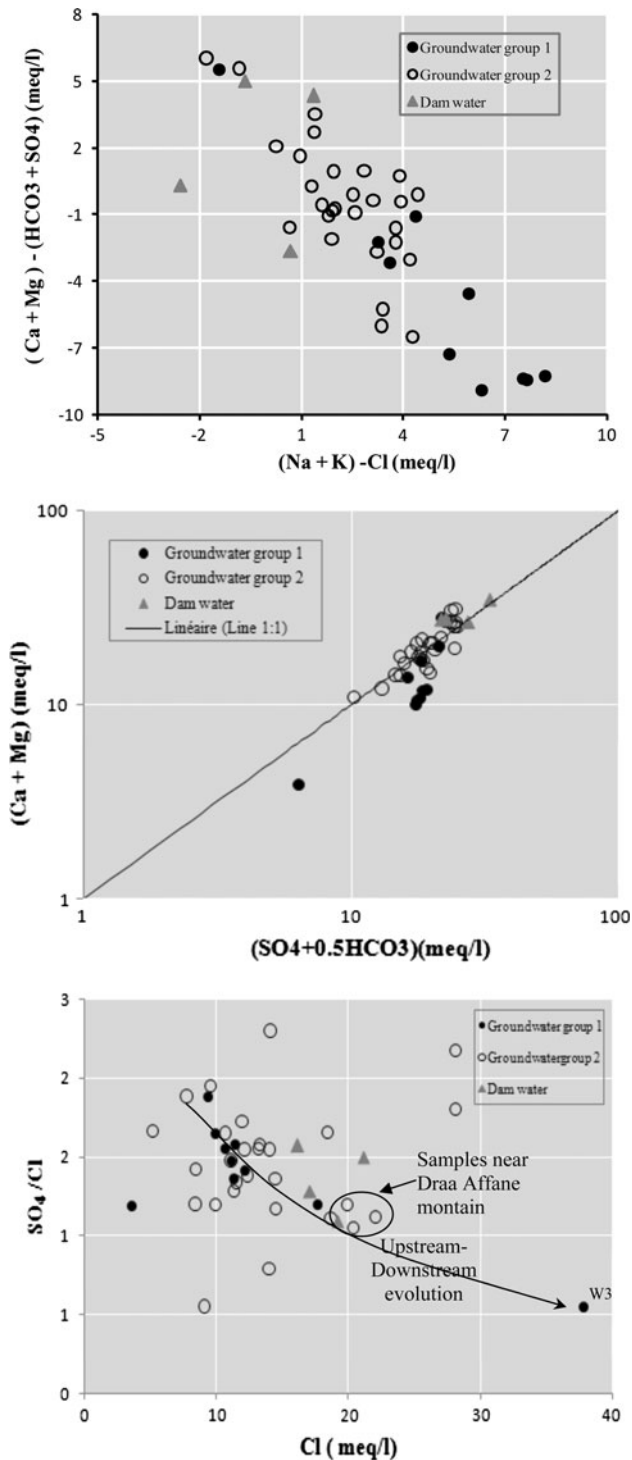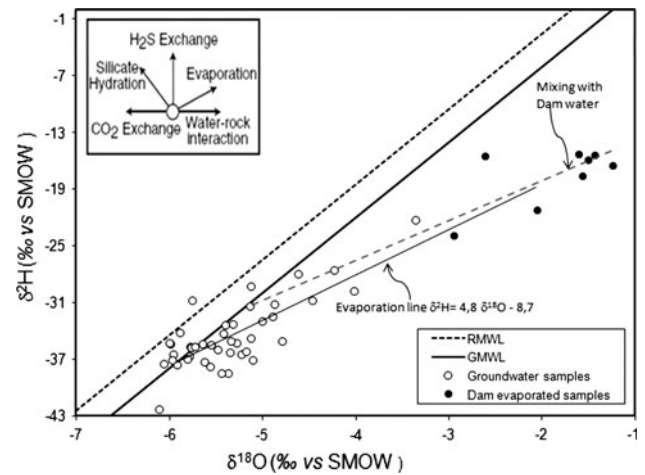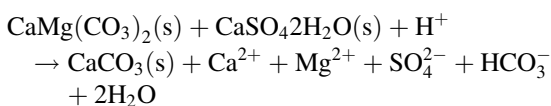he upstream of the basin and those characterized by a lower ratio are situated in downstream. However, some samples located near the Draa Aaffane Mountain (upstream of the basin) do not follow this general trend and indicate the influence of dissolution of anhydrite and/or gypsum outcrops.

Isotopic study

Stable isotopes ($\delta^{18}O$ and $\delta^{2}H$)

Deuterium and oxygen-18 stable isotopes provide important information on water origin, recharge under different climatic conditions and mixing of waters from different sources (Carol et al. 2009). In the conventional diagram of $\delta^{18}O/\delta^{2}H$, groundwater samples were plotted with respect to the precipitation input function represented by the Global Meteoric Water Line (GMWL: $\delta^{2}H = 8 \delta^{18}O + 10$) and the Local Meteoric Water Line (LMWL: $\delta^{2}H = 8\delta^{18}O + 11$) (Gay 2004; Jeribi 2004; Ben Ammar 2007). In this diagram, three groups of groundwater can be distinguished (Fig. 13).

Fig. 12 Plot of Cl versus (SO$_4$/Cl), Plot of (Ca + Mg) versus (SO$_4$ + 0.5 HCO$_3$), (Na + K − Cl)/(SO$_4$ + HCO$_3$) − (Ca + Mg) relationship

$$CaMg(CO_3)_2(s) + CaSO_4 2H_2O(s) + H^+$$
$$\rightarrow CaCO_3(s) + Ca^{2+} + Mg^{2+} + SO_4^{2-} + HCO_3^-$$
$$+ 2H_2O$$

Table 2 In situ measurements, geochemical and isotopic data of Sidi Saad dam water

Sampling date	T (°C)	pH	EC (mS/cm)	TDS (mg/L)	pCO$_2$	Ca (meq/L)	Mg (meq/L)	Na (meq/L)	K (meq/L)	HCO$_3$ (meq/L)	CO$_3$ (meq/L)	Cl (meq/L)	SO$_4$ (meq/L)	NO$_3$ (meq/L)
Storage Mai 2005	25	8	4.99	3.49	−2.88	25.93	8.84	18.55	0	2.8	0	21.13	31.67	0
Storage mars 2008	21.5	7.58	4.15	2.91	−2.30	19.8	6.96	16.84	0	4	0	16.16	25.42	0
Site of articial recharge mai 2005	26.1	7.8	3.87	2.71	−2.90	20.55	7.06	18.53	0	1.6	0	19.2	21.01	0
Site of articial recharge mars 2008	21	8	3.89	2.72	−3.14	20.84	6.99	18.43	0	1.6	1.4	17.09	21.9	0
Storage September 2009		7.01	3.93	3.13		19.82	8.33	19.66	0.013	1.64	0	17.3	28.85	0
Storage November 2009		8.15	3.94	3.19		20.54	8.61	20.06	0.399	1.51	0	17.71	30.12	0
Storage April 2009		8.02	3.96	3.22		18.74	8.39	21.01	0.535	1.97	0	16.34	27.64	0
Storage June 2009		7.53	4.06	3.03		16.31	7.68	15.93	0.178	1.47	0	17.16	25.28	0.02
Storage October 2009		7.46	4.03	3.22		19.78	8.37	20.35	0.468	1.8	0	16.16	31.23	0
Storage July 2009		7.35	3.75	3.11		22.09	7.92	18	0.275	1.97	0	15.11	28.96	0.04
Storage march 2009		7.94	4.11	3.27		21.1	8.62	21.01	0.276	1.47	0	17.03	29.28	0
Storage August 2009		7.05	3.84	3.26		24.33	7.74	20.76	0.411	2.29	0	17.17	26.13	0.08
Storage may 2009		8.11	3.96	3.00		22.83	8.62	21.14	0.284	1.8	0	16.32	28.63	0

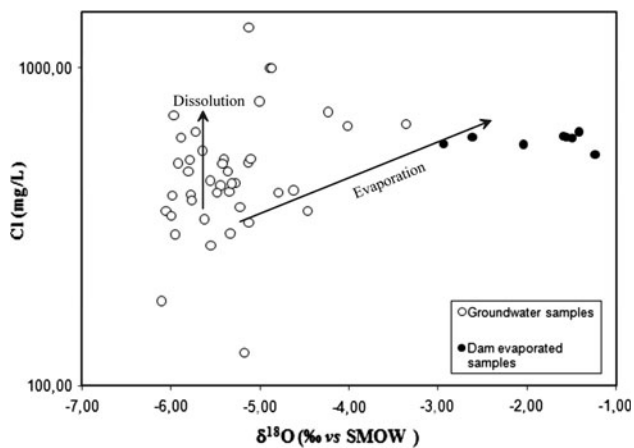| Sampling date	(‰ vs. SMOW)		SI					
	^{18}O	^{2}H	Calcite	Aragonite	Dolomite	Gypsum	Anhydrite	Halite
Storage Mai 2005	−1.56	−13.44	0.08	−0.06	−0.73	−0.16	−0.38	−5.19
Storage mars 2008	−1.82	−15.54	0.16	0.02	−0.56	−0.3	−0.52	−5.33
Site of articial recharge mai 2005	−1.54	−13.20	−0.2	−0.34	−1.28	−0.35	−0.57	−5.22
Site of articial recharge mars 2008	−1.51	−13.95	−0.19	−0.34	−1.29	−0.33	−0.55	−5.26
Storage September 2009	−1.60	−15.37	−0.24	−0.39	−0.74	−0.27	−0.49	−5.24
Storage November 2009	−1.43	−15.48	−0.27	−0.41	−0.80	−0.25	−0.47	−5.23
Storage April 2009	−2.94	−23.95	−0.18	−0.33	−0.59	−0.31	−0.53	−5.24
Storage June 2009	−2.61	−15.51	−0.35	−0.49	−0.90	−0.37	−0.59	−5.33
Storage October 2009	−2.05	−21.22	−0.21	−0.36	−0.68	−0.25	−0.47	−5.26
Storage July 2009	−1.23	−16.52	−0.12	−0.26	−0.56	−0.23	−0.45	−5.34
Storage march 2009	−1.50	−15.98	−0.26	−0.41	−0.80	−0.25	−0.47	−5.22
Storage August 2009	−1.57	−17.62	0.00	−0.14	−0.38	−0.24	−0.46	−5.22
Storage may 2009	−0.36	−13.47	−0.14	−0.29	−0.59	−0.23	−0.45	−5.24

Fig. 14 δ^{18}O/Cl diagram

The first group comprises wells influenced by dam water, located near the injected site of artificial recharge. These samples, which have a strong sulphate contents (1,000 mg/l), are characterized by the more enriched δ^{18}O and δ^2H contents. This may indicates the significance role of the artificial recharge by dam water (Table 2).

The second group includes groundwater samples that deviate from the GMWL with a regression line of δ^2H = 4.8δ^{18}O-8.7. This suggests a low enrichment by evaporation, which is probably the consequence of the infiltration of an evaporated component likely deriving from the return flow of irrigation water. However, this enrichment is very low compared to samples of the first group. This is probably related to the pivot irrigation practices, largely used in this studied area, that make the contact of water with the atmosphere lower than other irrigation practices, particularly flood irrigation. The spatial distribution of δ^{18}O contents shows that the second group corresponds to groundwater samples collected from the area of potential agricultural activity located in the Menzel Mhiri region. In this area, where irrigation is applied at a large scale, the excess of irrigation water undergoes excessive evaporation at the ground surface and in the vadose zone and returns to the aquifer with an evaporated signature.

The third group observed in the δ^{18}O/δ^2H diagram involves the rest of groundwater samples. These samples cluster, in the majority, between the GMWL and the LMWL, exhibiting depleted oxygen-18 and deuterium contents, which may indicate that the Zeroud aquifer is recharged by rainfall waters deriving from a mixture of Atlantic and Mediterranean air masses produced in high altitude.

A plot of chloride contents versus oxygen-18 (Fig. 14) shows the different process responsible for the salinity variation of groundwater in the studied area. Indeed the mineralization of the Zeroud aquifer is controlled by both

the dissolution and evaporation process. In fact, the major part of groundwater samples shows that chloride concentrations are not clearly correlated with the oxygen-18 contents, which suggest that their mineralization is mainly controlled by the dissolution of evaporate deposits. The well-defined relationship between the chloride and the 18 oxygen concentrations for some samples provides evidence about the existence of the evaporated groundwater near the injection site of the artificial recharge and in the Menzel Mhiri irrigated area.

Conclusions

The combination of major elements geochemistry and stable isotopes (δ^{18}O, δ^2H) has provided basic information about groundwater origin, hydrodynamic functioning and mineralization processes that control chemical composition in the Zeroud basin.

The hydrochemical investigation permits classification of the groundwater samples into two main water types: Na–Cl–SO$_4$ and Ca–SO$_4$–Cl. These water types are the result of the dissolution of halite, anhydrite and gypsum, reverse cation exchange and the dedolomitization process. In addition to these natural processes, return flow of irrigation waters, which are related to agricultural practices, and the artificial recharge from the dam reservoir water play important roles in the salinization of groundwater in the studied area. The isotopic tracing of the Zeroud aquifer highlights three recharge origins: The first significant recharge origin is related to the direct infiltration of actual meteoric water, particularly in the upstream of the basin. This is observed in the foothills bordering the basin and in the vicinity of the Zeroud Wady. The second recharge origin is insignificant and is from water that shows a high evaporation effect, which is related to the artificial recharge from dam reservoir water. Some groundwater samples show a relatively enriched oxygen-18 and deuterium contents. This enrichment is interpreted as an evaporative influence, indicating slow infiltration of return flow of relatively evaporated irrigation water.

References

Appelo C, Postma D (1993) Geochemistry, groundwater and pollution. A.A. Balkema, Rotterdam

Beartschi P (1976) Absolute 18O content of standard mean ocean water. Earth Planet Sci Lett 31:341

Bedir M (1995) Mécanismes géodynamiques des bassins associés aux couloirs de coulissements de la marge atlasique de la Tunisie Seismo-statigraphie, seismo-tectonique et implications pétrolières. Ph D es-sciences. Fac. Sc. Tunis, Tunisia

Bel Haj Salem S (2006) Recharge artificielle de la nappe de la plaine du Kairouan par les lâchers du barrage Sidi Saad: Etude isotopique et géochimique. Mastère, National School of Engineers, Sfax, Tunisia

Ben Ammar S (2007) Contribution à l'étude hydrogéologique, géochimique et isotopique des aquifères de Ain El Beidha et du bassin du Merguellil (plaine de Kairouan): implications pour l'étude de la relation barrage-nappes. Thèse doctorat, université de Sfax, 2007

Bouzaiane S, Laforgue A (1986) Monographie hydrologique des oueds Zeroud et Merguellil. Direction Générale des Ressources en Eau en Tunisie (DGRE) en coopération avec l'institut de Recherche scientifique pour le développement (ORSTOM). Prog Dacti, 1100 p

Carol E, Kruse E, Mas-Pla J (2009) Hydrochemical and isotopical evidence of ground water salinization processes on the coastal plain of Samborombón Bay, Argentina. J Hydrol

Dassi L (2004) Etude hydrogéologique, géochimique et isotopique du système aquifère du bassin de Sbeitla (Tunisie Centrale). Thèse, University Sfax, Tunisie

Epstein S, Meyada TK (1953) Variations of 18O content of waters from natural sources. Geochim Cosmochim Acta 4:213–224

Gay D (2004) Fonctionnement et bilan de retenues artificielles en Tunisie: Approche hydrochimique et isotopique. Thèse de Doctorat, Université de Paris XI, Paris, France

Jeribi L (2004) Caractérisation hydrochimique et isotopique des eaux du système aquifère du bassin de Zeroud (Plaine de Kairouan, Tunisie Centrale). Thèse de Doct. 3ème cycle, Fac. Des sciences de Tunis

Mokrik R, Petkevièius R (2002) Baltijos baseino Ðventosios—Arukiulos, franio ir apatinio karbono-famenio kompleksø paleo-hidrogeologine¨ raida. Litosfera 6:48–58

Nazoumou (2002) Impact des barrages sur la recharge des nappes en zone Aride: Etude par modélisation numérique sur le cas de Kairouan (Tunisie centrale). Th, Doct, ENIT, Tunis, Tunisie

Parkhurst D, Appelo CAJ (1999) User's guide to PHREEQC (Version 2)—a computer program for speciation, batchreaction, one-dimensional transport, and inverse geochemical calculations. US Geol Surv Water Resour Inv Rep: 99–4259, 310 p

Piper AM (1944) A graphic procedure in the geochemical interpretation of water analyses. Trans Am Geophys Union 25:914–923

Thatcher LL, Janzer VJ, Edwards RW (1977) Methods for determination radioactive substances in water and fluvial sediments. In: Techniques of water resources investigations. US Geological Survey Washington, pp 79–81

Yaich C (1984) Etude géologique des chaînons du Chérahil et du Kherchem el Artsouma (Tunisie centrale). Liaison avec les structures profondes des plaines adjacentes. Thèse de 3 ème cycle Fac. Sc. et Tech. De l'université de Franche-comté. Besançon